3D DESIGN, CONSTRUCTION, AND FIELD ANALYSIS OF CIS MAIN DIPOLE MAGNETS

G. P. A. Berg, W. Fox, D. L. Friesel, and T. Rinckel
Indiana University Cyclotron Facility, 2401 Milo B. Sampson Lane, Bloomington, IN 47405

Abstract

Four normal conducting main dipole magnets were designed and built for the Cooler Injector Synchrotron CIS allowing proton acceleration up to 220 MeV with a magnetic field of $B_{max} \approx 1.78$ T. Field calculations in two (2D) and three (3D) dimensions were used to optimize magnet laminations and end packs. Endpacks are designed to determine edge angle, effective field length (EFL) and to compensate hexapole components. The magnets are assembled of machined laminated wedges to accommodate the strong curvature. Field maps were performed in the range of B = 0.25 T - 1.8 T. The magnet parameters are well within expected specifications and initial tests at injection energy of CIS were conducted successfully.

1 INTRODUCTION

The main objective of CIS [1] is to replace the present Cyclotron injection to fill the IUCF Cooler up to about 10^{11} protons within a few seconds. The CIS circumference of 17.384 m allows bucket-to-bucket injection into the Cooler. The lattice for CIS requires four laminated 90° main dipole magnets with bending radius ρ = 1.273 m, EFL = 2 m, and edge angles of 12°. Initial operation of 1 Hz, with later upgrade to 5 Hz is planned and eddy current effects were taken into account.

With the availability of improved finite element electromagnet design programs [2] with 3D capability, faster computers and new materials for magnet construction it has become feasible to design magnets optimized for special purposes without costly and time consuming prototyping. This has allowed us to design high field dipole magnets for a very compact and cost efficient synchrotron. Despite the best field calculations there are remaining uncertainties in the produced magnets resulting from uncertainties in materials, fabrication, construction details and other approximations which cannot be or which are impractical to be modeled in the calculations.

We adopted the following guide lines for the design.

1) Consider and determine construction methods.

2) Calculate axisymmetric radial sections to determine the laminations and to evaluate higher order components inside the magnet. Evaluation of dynamical aperture for magnet without end effects.

3) Study end block parameters using 2D calculations.

4) Compensate hexapole components developing along the magnet and at the ends by designing final end blocks using 3D calculations.

5) Model complete magnet in 3D and verify dynamical aperture using field integrals $\int Bdl$ along beam rays.

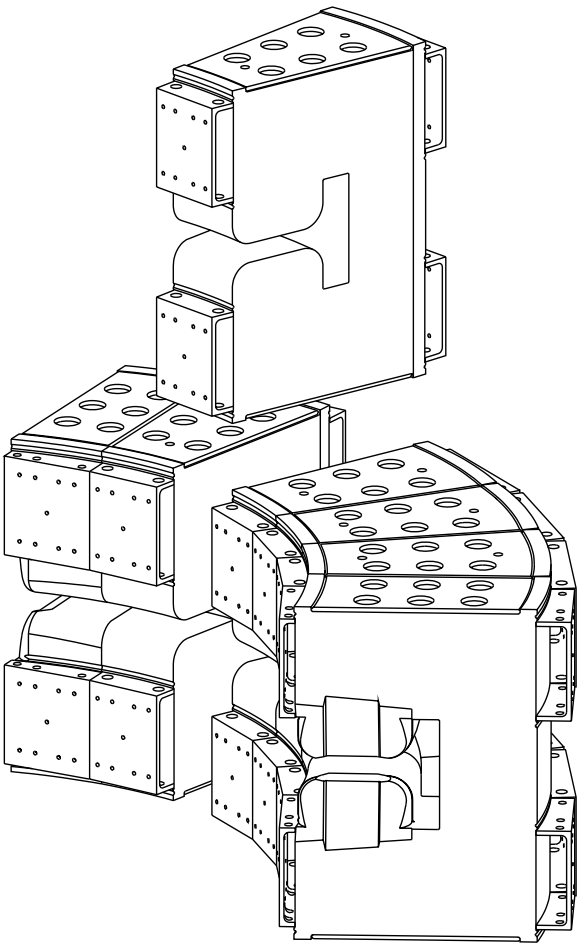

Figure 1: Isometric plot of CIS dipole magnet assembly. For better viewing one wedge is moved up and the coil is removed.

2 MAGNET DESIGN AND CONSTRUCTION

For cycling rates up to 5 Hz lamination thickness of 1.519 mm was found to be sufficient. The large bend of 90° prevented application of usual stacking methods. We decided to stack and cure lamination blocks and machine appropriate wedges, assembled as shown in Fig. 1. This was possible because of the availability of B-stage epoxy, which is dry and allows stacking of large blocks which is not possible using the wet-laying method. Bonding of the B-stage epoxy is done subsequently by curing at 150°. The electrical insulation is also provided by the epoxy. We decided to build C-magnets because of several potential problems with H-frame magnets in this design, e.g. field distortions from lamination severely cut at the thin side of the wedge.

The magnet consists of five machined wedges and two

0-7803-4376-X/98/$10.00

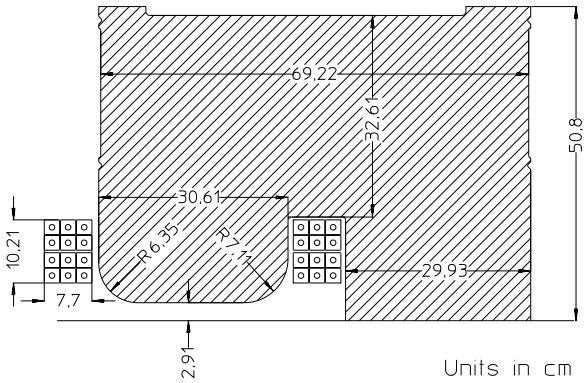

Figure 2: Upper half of CIS lamination and coil cross section.

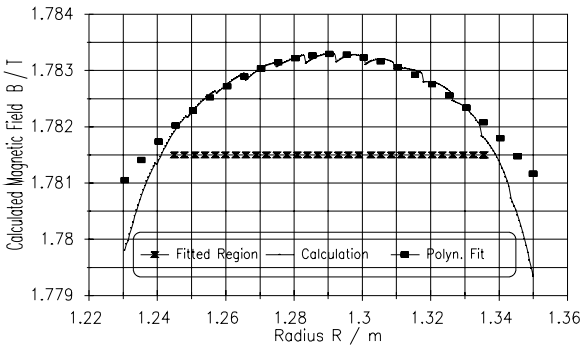

Figure 3: Axisymmetrical field calculation at high field and fit.

end blocks. The pole piece ends show a Rogowsky profile in the center and extrusions ("noses") at the sides. Plates and U-shaped brackets were welded on the bocks for mechanical stability. While the five inner wedges are welded together at the joining brackets, the end blocks are bolted to the assembly for easy removal if necessary. Not shown in Fig. 1 is the strong support to which all block are bolted. No prototyping was done except for one initial end block which was slightly remachined with simple cuts at the "noses" for optimization. A low carbon soft steel with B = 1.8 T at H = 72 Oe was chosen to provide a high saturation limit. The coercive force of about 3.1 Oe was acceptable for our application with hysteresis losses below approximately 1 kW per magnet for the acceleration of protons up to 220 MeV at 5 Hz. The steel was cold rolled in a continuous process and came from a single steel ingot. This eliminated otherwise necessary randomization of laminations during stacking.

In the final calculations we used a B(H) curve deduced from measurements with an Epstein facility for the actual material purchased. Fig. 2 shows the lamination geometry. Also shown are cross sections of the coils which consist of two pancakes with 6 windings in two layers. The pancakes fit through the vertical gap of g = 5.82 cm for assembly. Maximum current is 4.2 kA.

3 AXISYMMETRIC FIELD CALCULATIONS

The lamination geometry was optimized using axisymmetrical field calculations with the finite element code MagNet which solves the Laplace equation in 2D and 3D geometries. We optimized the size of the return, inner and out radii of the sides of the pole pieces R = 6.35 cm and 7.11 cm, respectively and the location of the coils slightly above the midplane to avoid eddy current effects from fringe fields in the coil conductor. We compared the circular pole edges and a Rogowsky profile and found that in saturation the circular profile provides a 1 - 2 cm wider good-field region. Shims on the pole pieces in the gap were found to be inefficient at high fields and are therefore not used.

Calculations were performed in the field range from B = 0.34 - 1.78 T. The field as function of the radius ρ in the midplane was fitted by the lower terms of a Taylor series $B(x) = B_0 + B_1(x\text{-}x_0) + 1/2B_2(x\text{-}x_0)^2 + 1/6B_3(x\text{-}x_0)^3$. Field calculation and fit at a high excitation are shown in Fig. 3. The range of 9 cm from radius ρ = 1.245 m to 1.335 m was used in the fit. The fitting results are x_0 = 1.291 m, B_0 = 1.7833 and B_2 = -1.22277 T/m_2

No improvement of the χ^2 could be achieved by including quadrupole B_1 and octupole B_3 components except for a small $B_1 < 0.00035$ T/m for the lowest fields. Therefore these terms where omitted in all fits. Also the inclusion of a B_4-term and higher order terms was not necessary in the fitted range of 9 cm.

The fitting results of $k2 = B_2/B\rho$ for all calculations are summarized below in Fig. 6 denoted by the label "Axisym". The hexapole component k2 is negative and quite constant up to about 1.5 T when saturation effects set in as visible in Fig. 3.

4 2D AND 3D ENDPACK CALCULATIONS

The end blocks of the magnet assembly are parallel blocks of bonded laminations but required machining of the pole piece ends to adjust EFL, edge angle and hexapole component. Around the central ray a Rogowsky profile in beam direction (see Fig. 1) was chosen to provide an effective field boundary EFB close to the mechanical length of the pole pieces. The effect of the "noses" were studied in 3D calculations and edge angle and hexapole components were optimized. The $\int Bdl$ is the field quantity which determines the path of the circulating particles. We analyzed the calculated 3D field in the midplane of the magnet and calculated $\int Bdl(\rho)$ as function of radius ρ. The calculated $\int Bdl(\rho)$ values were compared to the same quantity of an ideal magnet with a constant field within the EFB and zero field outside. This allowed us to define the average quantities of hexapole, EFL and edge angle shown in Figs. 4,5, and 6.

The average hexapole k2 calculated in this way is plotted in Fig. 4 as solid line and labeled "Endpack". The effect of the hexapole component "Axisym" inside the magnet is compensated to better than $|k2| < 0.1\ m^{-3}$ up to a field of about 1.4 T. Then k2 becomes more negative due to saturation effects and is about k2 = - 0.55 m^{-3} at 1.8 T field.

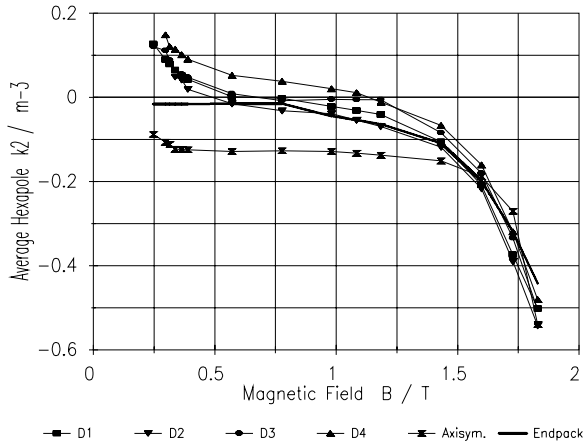

Figure 4: Hexapole component as function of field B.

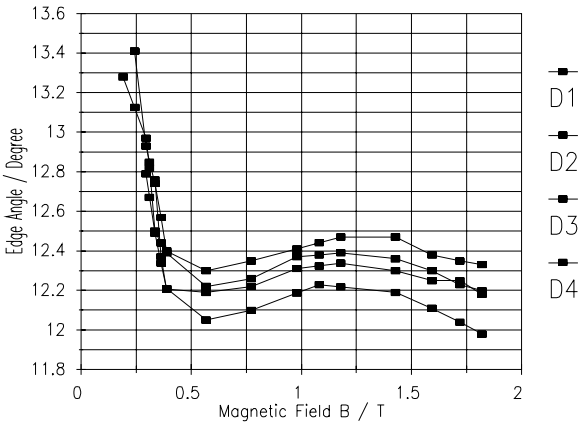

Figure 6: Edge angle as function of magnetic field B.

5 FIELD MEASUREMENTS AND ANALYSIS

The fields of all four dipole magnets were mapped with a 16 Hall probe array mounted on the arm of a large x-y table. All Hall probes were calibrated relative to each other within about 10^{-4} precision. Absolute calibration was established by comparison to NMR probe measurements to similar precision. Midplane measurements were taken on a 1.27 cm Cartesian grid inside the gap and about 40 cm outside in beam direction for several excitations. Analysis of relevant parameters from the data are performed in the same way as for the calculations. Results for dipoles D1-4 are shown in Figs. 4 - 6. All measured quantities

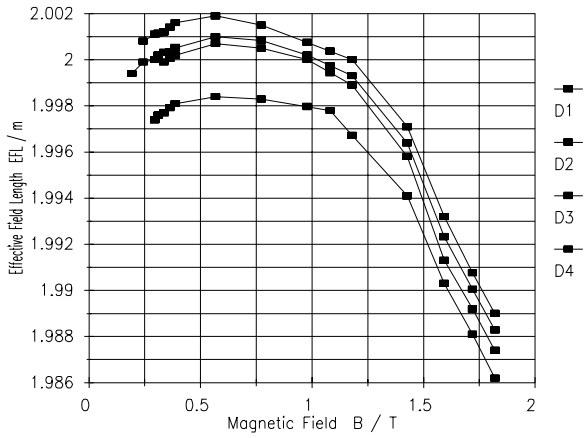

Figure 5: Effective field length as function of magnetic field B.

show some deviation which can be expected from uncertainties in the manufacturing process. The calculated and measured hexapole component shown in Fig. 4 agrees well within manufacturing uncertainties except for a rise of k2 $\approx 0.1\ m^{-3}$ at or slightly below injection field. The effect of the end pack compensation is clearly visible at fields up to 1.5 T. The EFL shown in Fig. 5 agrees within the thickness of one lamination well with the design value of 200.0 cm up to a field of about 1.2 T. For higher fields the EFL decreases by about 1 cm for the highest field of 1.8 T.

In Fig. 6 the edge angle is shown. The average value is about 12.25° slightly higher than the design value of 12° for fields higher that 0.35 T. This could be corrected in the magnet design but was not done because it can be compensated easily with the trim quadrupoles, as mentioned before. An increase at lower fields is observed and several measurements were taken below injection field to study this effect, the nature of which is not understood.

6 CONCLUSIONS AND SUMMARY

The four normal conducting CIS main dipoles with several new design and construction methods perform as designed and were tested at injection energy for CIS. Detailed field measurements and analysis show that these magnets will enable the synchrotron to operate up to about 220 MeV just below the transition energy of the present lattice design.

7 ACKNOWLEDGEMENTS

We want to acknowledge the advise and help, which we received from Fermilab, Brookhaven National Laboratory, the Advanced Photon Source, and the Budker Institute of Nuclear Physics, Novosibirsk which has enabled us to find quickly a successful design for our dipole magnets. We also would like to thank the technical staff of IUCF for their assistance in all stages of the project.

8 REFERENCES

[1] Conceptual Design Manual for CIS, Internal Report, Indiana University Cyclotron Facility, Jan. 30, 1995.

D.L. Friesel and S.Y. Lee, "Status of the IUCF Cooler Injector Synchrotron", this publication.

[2] In this design we used the computer code MagNet, Infolytica Corp., Montreal, Quebec.

D.A. Lowther, P.P. Silvester, Computer Aided Design in Magnets, Springer-Verlag, New York 1986.